Materials Research Express

PAPER

Thermally synthesized MnO nanoparticles for magnetic properties and lithium batteries

Materials Research Express

PAPER

Thermally synthesized MnO nanoparticles for magnetic properties and lithium batteries

RECEIVED
5 September 2018

REVISED
10 October 2018

ACCEPTED FOR PUBLICATION
30 October 2018

PUBLISHED
9 November 2018

Ying Zhang[1], James D Steiner[2], Jaylon Uzodinma[1], Julia Walsh[2], Benjamin Zydlewski[2], Feng Lin[2], Ying Chen[1], Jinke Tang[3], Nihar Pradhan[1] and Qilin Dai[1]

[1] Department of Chemistry, Physics, and Atmospheric Science, Jackson State University, Jackson, Mississippi 39217, United States of America
[2] Department of Chemistry, Virginia Tech, Blacksburg, Virginia 24061, United States of America
[3] Department of Physics & Astronomy, University of Wyoming Laramie, Wyoming 82071, United States of America

E-mail: qilin.dai@jsums.edu

Keywords: MnO nanoparticles, ferromagnetic behavior, lithium ion battery

Supplementary material for this article is available online

Abstract

MnO nanoparticles have drawn much attention due to their potential applications in spintronics and energy storage. In this work, we used a thermal decomposition method to synthesize MnO nanoparticles, and we controlled the reaction temperature and Mn(II):oleylamine:oleic acid ratios to obtain varied sizes ranging from 90 nm to 800 nm. The prepared MnO nanoparticles were characterized by x-ray diffraction (XRD) and Scanning electron microscopy (SEM). Magnetic measurements (M-H loops and M-T curves) were used to study the magnetic properties of the prepared MnO nanoparticles. The results showed that surface defects caused surface anisotropy that resulted in low temperature ferromagnetic behavior of the nanoparticles (90 nm–220 nm). The coercivity of 1500 Oe were obtained. The synthesized MnO nanoparticles were also studied as anode materials in lithium ion batteries, and achieved very promising results.

1. Introduction

In recent years, transition metal oxide nanoparticles have attracted research attention due to their special structures, magnetic behaviors, luminescence properties, and reaction activities [1–7]. Among all the transition metal oxides, manganese oxide nanoparticles are one of the most promising candidates toward spintronics and energy storage applications [8, 9]. Additionally manganese oxide nanoparticles have potential applications in catalysis [10], magnetic resonance imaging (MRI) agents [11], cancer treatment [11], drug delivery [12], and biosensors [13]. Size and shape play a critical role in the electrical and magnetic properties; therefore, it is critical to synthesize and study MnO nanoparticles in different shapes and sizes. Several synthetic methods of MnO nanoparticles have been developed: vapor deposition [14], sol-gel method [15], hydrothermal method [16], electro-deposition [17] and thermal decomposition [10, 18]. Chiang *et al* reported a thermal decomposition method that used bulk MnO and oleic acid at 305 °C to prepare MnO 6–32 nm nanoparticles. They exhibited ferromagnetic behavior below blocking temperature at 28.8 ∼ 22.1 K [19]. Rao *et al* reported the synthesis of MnO particles by thermal decomposition of $Mn(acac)_2$ in oleylamine and water where adjust the reaction temperature (220 °C–250 °C) and time (3 h–9 h) resulted in nanoparticles between 11 and 22 nm. Lee *et al* reported thermal decomposition of $Mn_2(CO)_8$ vapors with a resistive heater at 400 °C–450 °C to obtain MnO nanoparticles of 6–14 nm [20]. Most of these methods required very special starting materials, such as $[Mn(acac)_2]$, $Mn_2(CO)_8$ or elevated temperatures (400 °C–450 °C). Zhang *et al* developed a thermal decomposition method using manganese (II) acetate in a ligand mixture of oleylamine, oleic acid and 1-octadecene [21]. A mixture phase of MnO and Mn_3O_4 was obtained in their work [21].

MnO nanoparticles have been reported to show ferromagnetic behavior opposed to the antiferromagnetic properties in bulk phase. Lee *et al* reported that the MnO 5–10 nm nanoclusters show ferromagnetic behavior

Table 1. Sample information.

Menganese(II) Acetate tetrahydrate: OA:OL(mol:mol:mol)	Temperature (°C)	Sample name	Size, morphology
2:6:6	220	S1	90 nm, octahedron
2:6:6	250	S2	190 nm, octahedron
2:6:6	280	S3	280 nm, octahedron
2:6:6	310	S4	290 nm, octahedron
1:6:6	280	S5	220 nm, octahedron
4:6:6	280	S6	270 nm, octahedron
8:6:6	280	S7	800 nm, octahedron
2:6:0	280	S8	100 nm, octahedron
2:6:3	280	S9	110 nm, octahedron
2:6:12	280	S10	670 nm, octahedron

with a phase transition from a ferromagnetic to a paramagnetic phase at 27 K due to cluster size effect or surface spin effect [20]. Hyeon *et al* studied the magnetic properties of MnO nanorods, and found that the nanorods with the size of 7 nm × 33 nm showed two blocking temperatures at 35 K and 280 K respectively [18]. Park *et al* also reported that MnO 5–22 nm nanoparticles showed weak ferromagnetic behavior at low temperature (10–25 K). They claimed that uncompensated surface spins on an antiferromagnetic core of MnO nanoparticles caused this behavior. Therefore, the size effect provides an explanation to the ferromagnetic properties of MnO.

Furthermore, MnO nanoparticles have been an exciting candidate for lithium ion battery (LIB) anodes, due to their high theoretical specific capacity (756 mAh g^{-1}), abundance in nature, environmental friendliness, non-toxicity, and high thermal stability [22]. Additionally, MnO has a variety of structure types that allow for a diverse selection of materials [23].

In this work, we report a method to synthesize MnO nanoparticles (e.g., octahedron structure) by thermal decomposition of manganese (II) acetate in a mixture of oleylamine and oleic acid under the protection of nitrogen gas. We modified Zhang's method by increasing the reaction solution concentration and eliminating the 1-octadecene ligand [21]. MnO nanoparticles without any additional phases were obtained in this work. The resulting octahedron nanostructure, ranging from 90 nm to 800 μm, were synthesized and by controlling the reaction temperatures and the ratios of Mn(II) to ligands. We observed that the ferromagnetic behavior of MnO nanoparticles with the size of 90 and 220 nm at low temperature, which can be ascribed with surface anisotropy due to the crystal-field splitting and level occupancy caused by surface defects. The applications of these MnO nanoparticles in LIBs were studied, and we observed that smaller MnO nanoparticles perform better as anode materials than larger particles.

2. Experimental section

2.1. Synthesis of MnO nanoparticles

The thermal decomposition under nitrogen of manganese (II) acetate tetrahydrate (HIMEDIA) in the presence of organic ligands oleylamine (OA) (TCL) and oleic acid (OL) (Alfa Aesar) was used to synthesize the MnO nanoparticles. All the chemicals were utilized directly without further purification. The mixture of manganese (II) acetate tetrahydrate, OA and OL, with varied ratios, was heated to 120 °C under stirring. The solution was then degassed and purged with nitrogen gas for three times. Then, the mixture was heated at a designated temperature under stirring for 2 h. The resulting solution was cooled to room temperature naturally. The products were purified and washed with toluene and methanol 5 times. MnO nanoparticles were obtained by drying under vacuum at 50 °C for 24 h. To control the size of MnO nanoparticles, we adjusted the reaction conditions, including temperature and the manganese (II):ligands ratios. The synthesis parameters and sample information are shown in table 1.

2.2. Electrode preparation

Electrodes were prepared using 80% active material (MnO), 10% polyvinylidene fluoride, and 10% acetylene carbon black in N-methyl-2-pyrrolidinone and then cast onto carbon coated aluminum foil current collectors. The electrodes were dried under vacuum at 120 °C. CR2032-type coin cells were assembled in an argon-filled glovebox using the electrode as the cathode and lithium metal as the anode. The cathode and anode were separated with a glass fiber separator which was soaked with an electrolyte of 1 M LiPF6 dissolved in a 3:7 ratio of EC/EMC with 2 wt% VC.

2.3. Measurements

Powder XRD results were collected with a Rigaku Smart Lab x-ray Diffractometer. Scanning electron microscopy (SEM) images were taken by Scanning Electron Microscopy TESCAN LYRA3. The magnetic hysteresis (M-H) loops of the produced MnO nanoparticles were measured on a Physical Properties Measurement System (PPMS) from Quantum Design. All the electrochemical testing was performed using a LAND battery testing system. 1 C was defined as fully charging the material in one hour, with a specific capacity of 756 mAh g^{-1}. The same rate was used for discharging the cathode.

3. Results and discussion

3.1. Structural properties

OA and OL have been reported as functional ligands for nanoparticle synthesis due to their size and crystal structure facet control capabilities. We used x-ray diffraction (XRD) to characterize the crystal structure of the produced MnO nanoparticles. The diffraction peaks indicate that all of the samples are pure MnO with octahedron structure (JCPDS 07-0230) (figure S1 is available online at stacks.iop.org/MRX/6/025015/mmedia). To study the influence of synthesis conditions on the MnO nanoparticle growth, the SEM images showed that all the prepared MnO nanoparticles exhibit octahedron morphology(figure 1). Figures 1(a)–(d) demonstrated that the temperature-dependent SEM images of S1, S2, S3 and S4 had average sizes of 90 nm, 190 nm, 280 nm and 290 nm, respectively. This indicated that the sizes increased with increasing temperature. This trend is consistent with our previous ZnO nanoparticles results [24]. It is believed that temperature affects particle growth, specifically during late stage of condensation – Ostwald ripening through interfacial energy, growth rate coefficients and equilibrium solubility. Nanoseeds formed at the initial stage of the reaction. Then the nanoseeds aggregated together to form nanoparticles. Higher temperature involved more nanoseeds aggregating together, which led to large nanoparticles. Figures 1(e)–(g) showed the SEM images of S5, S6 and S7 (figures 1(e)–(g) demonstrated that the average sizes of were 220 nm, 270 nm and 800 nm, respectively. Combining with sample S3, the average sizes of MnO nanoparticles are 220 nm, 280 nm, 270 nm and 800 nm as the ratios of Mn: OA: OL are 1:6:6, 2:6:6, 4:6:6 and 8:6:6 respectively. Therefore, the sizes of MnO increased with the increasing of Mn(II) concentration in the reaction solution. High concentration of source material will lead to the formation of more nanoseeds, and the nanoseeds will be much easier to aggregate with each other to produce large nanoparticles. These results are consistent with our previously work on $NiFe_2O_4$ nanoparticles [25]. The SEM images of S8, S9 and S10 (figures 1(h), (i)) demonstrated nanoparticle sizes of 100 nm, 110 nm, and 670 nm in conjunction with the ratios of Mn:OA:OL of 2:6:0, 2:6:3 and 2:6:10 respectively. The sizes of MnO nanoparticles; increased with the decreasing OA amount. Our previous work on ZnO:Mn nanocrystals showed similar results, where the sizes of ZnO:Mn decreased as the ratio of OA to OL ratio increased [24]. Sun *et al* also studied the synthesis of Fe_3O_4 nanoparticles with different ratios of OA to benzel ether, and observed that the sizes of Fe_3O_4 nanoparticles increased with OA to benzel ether ratio. Sun proposed that the oleylamine works as both a reducing agent and stabilizer, and the trend was attributed to the insufficiency of capping as the amount of OA decreased [26].

3.2. Magnetic properties

Figures 2(a) and (b) show The zero-field-cooled (ZFC) and field-cooled (FC) (100 Oe) of sample S5 (220 nm) and S1(90 nm). indicated a transition peak at ~27 K in ZFC runs (figures 2(a), (b)). Such a transition has been seen in MnO nanoparticles and corresponded to the blocking temperature of the superparamagnetic moments that originated from uncompensated surface spins [20, 27]. Generally, MnO nanoparticles with smaller sizes (<40 nm) have been reported to show such weak ferromagnetic behavior at low temperature. Park *et al* ascribed this behavior to uncompensated surface spins on the antiferromagnetic core of the MnO nanoparticles [28]. On the other hand, our results showed that large MnO nanoparticles also exhibited the weak ferromagnetism and superparamagnetic behavior. Since the blocking temperature was about the same as reported elsewhere [27], we hypothesized that the same surface anisotropy was behind the blocking of the superparamagnetic uncompensated surface spins. Meaning that the crystal-field splitting and level occupancy due to surface defects resulted in a large surface anisotropy in the MnO nanoparticles. Figures 2(c) and (d) showed the field-dependent magnetization M at different temperatures (5 K, 50 K and 300 K) for S5 and S1, respectively. For both, at temperatures above the blocking temperature (300 K and 50 K), the hysteresis loops showed a straight line, which can be attributed to the paramagnetic or superparamagnetic behavior as the temperature is above the Neel temperature of MnO. When the temperatures decreased to 5 K (below the blocking temperature), hysteresis loops showed a coercivity of 500 Oe and 1500 Oe for S5 and S1 respectively. Some previously published papers reported similar results with MnO nanoparticles and nanorods of sizes smaller than 30 nm [18, 19].

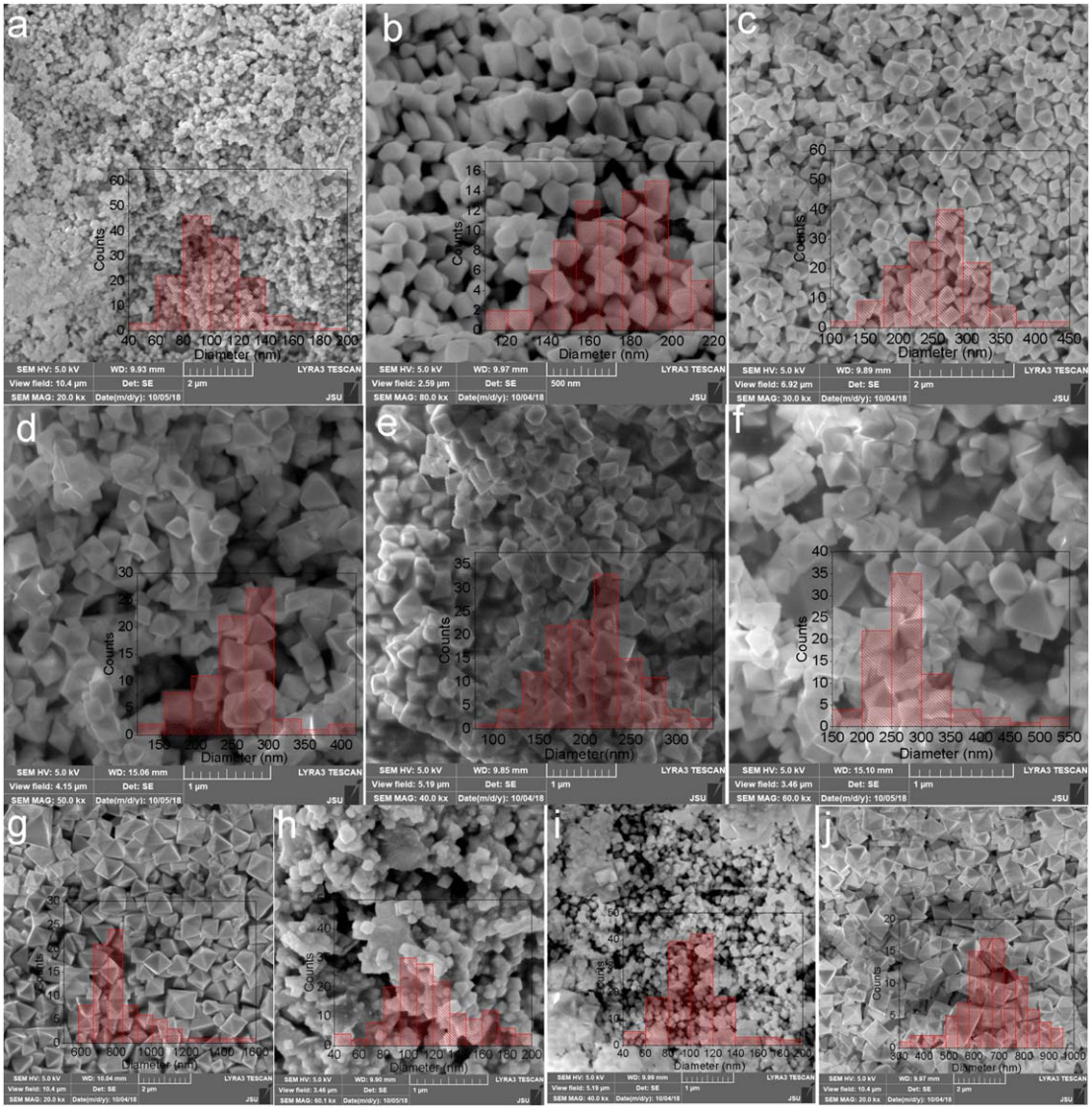

Figure 1. SEM images. (a): S1; (b): S2; (c): S3; (d): S4; (e): S5; (f): S6; (g): S7; (h): S8; (i): S9, (j): S10.

3.3. Application in lithium battery

We evaluated the battery performance of the S5 and S7 particles in lithium half cells (figure 3). The coin cell for S5 was run at C/5 with a theoretical charge capacity of 756 mAh g^{-1} (figure 3(a)). The material behaved in a similar pattern as a typical conversion anode. The initial specific charge capacity was ~301 mAh g^{-1} and rose to a maximum of ~428 mAh g^{-1} before fading to 291.1 mAh g^{-1}, which meant it maintained 96.7% of its capacity over 100 cycles. To further study this material, we performed a rate capability test to observe the effects of faster charging on the charge capacity (figure 3(b)). We observed a gradual increase in the specific charge capacity during the initial C/5 cycling. The specific charge capacity began at 298 mAh g^{-1} and rose to a maximum of ~412 mAh g^{-1}. Subsequently, we observed a decreased specific charge capacity at higher cycling rates and reached ~175 mAh g^{-1} at 2 C. Overall, the material maintained a capacity of ~389 mAh g^{-1}, which was a retention of 130.6% after 36 cycles of the rate capability test. By comparison, maintaining C/5 for 36 cycles had a retention of only 106.4% (figure 3(a)). Thus, the direct comparison indicated that the increased current densities limited some of the deterioration during the cycling of the anode material. Finally, for the S7 anode material, the specific charge capacity was lower than100 mAh/g and failed after 62 cycles. This implies that the size of the active particles could play a key role in the charge capacity of MnO particles. The smaller 220 nm particles resulted in a much better performance than the larger 800 nm particles. The capacity gradually increased in the initial cycles due to the activation period of active particles, for example, as the cycling continued, the electrolyte wetting became better. After that, a rapid fading behavior was observed. We conjecture that the fading was caused by the impendence buildup from the extensive passivation of the active particles. After the surface was sufficiently passivated, the impedance buildup slowed down, and the capacity became stable.

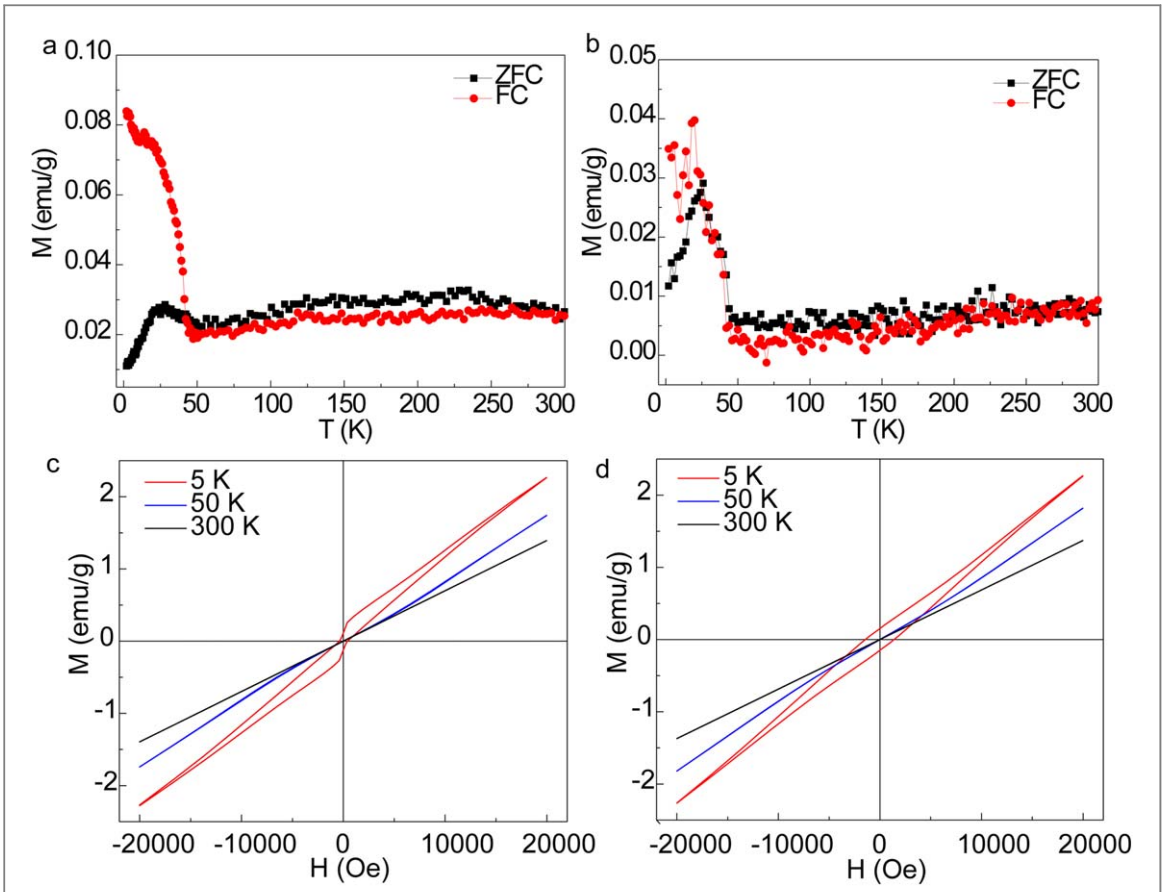

Figure 2. (a), (b): Temperature-dependent ZFC and FC (50 Oe) magnization (M) versus temperature (T) for a: S5 and b: S1; (c), (d): Field variation of magnetization at different temperatures for c: S5 and d: S1.

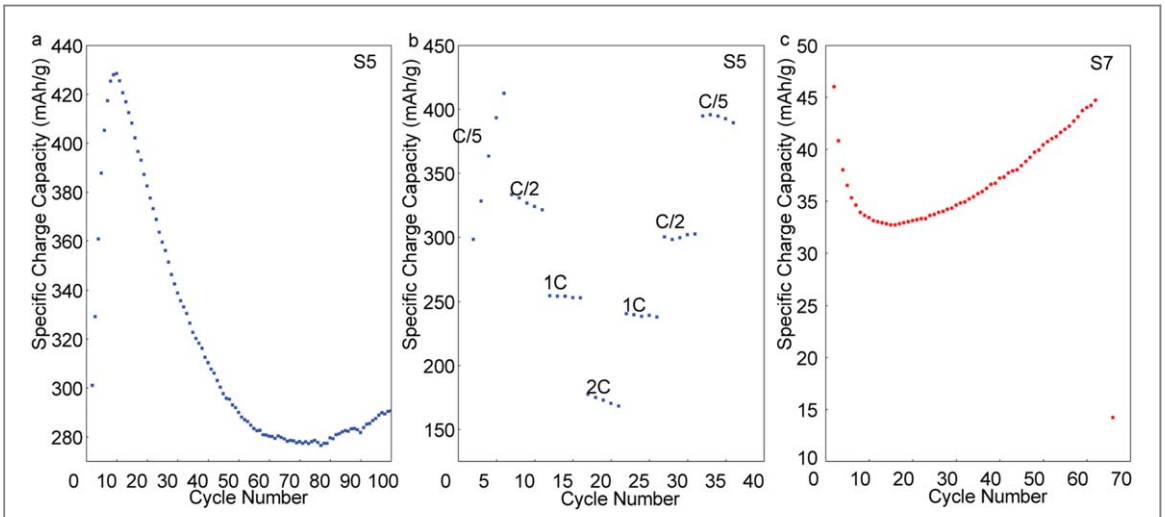

Figure 3. Electrochemical data for (a) 200 nm octahedron particles for 100 cycles at C/5, (b) rate capability test of the 200 nm material, and (c) 1 μm octahedron particles at C/5 charging rate.

To study the conductivity of the samples affected by the sizes, powder pellets were prepared by cold pressing (8 MPa). Four probe conductivity measurements were preformed to obtain the conductivity of the pellets. The conductivity of the samples versus sizes are shown in figure S2. The conductivity values of the samples with smaller sizes are of the order of 10^{-10} ohm^{-1} cm^{-1}. The conductivities of the samples with larger sizes (several hundred nm) show the order of 10^{-9} ohm^{-1} cm^{-1}, which is consistent with the literature about the bulk MnO [29]. Therefore, the conductivity increases with increasing particle size. The smaller conductivity values of small-sized samples can be attributed to the ligands and surface defects located on the surface, which play a role as

electron transport barriers to reduce the conductivity. The samples with larger sizes usually have less surface defects and less passivating ligands, leading to larger conductivity values.

4. Conclusion

In this work, we reported a thermal decomposition method to synthesize MnO nanoparticles with manganese (II) acetate in the presence of OA and OL under the protection of nitrogen gas. We analyzed the effects of synthesis parameters, including reaction temperatures, and the Mn(II) to ligand ratios on the MnO nanoparticle growth in terms of sizes. The prepared MnO nanoparticles with cubic crystal structure exhibited 90 nm to 800 nm nanooctahedrons. The magnetic properties of the prepared MnO nanoparticles were studied and demonstrated ferromagnetic behavior of MnO nanoparticles in relatively large sizes (90 nm −220 nm). We attributed this behavior to surface anisotropy in the MnO nanoparticles due to the crystal-field splitting and level occupancy caused by surface defects. The prepared MnO nanoparticles also were successfully applied as anode materials for lithium ion batteries, and we determined that the nanosized particles provided an initial capacity of 301 mAh g^{-1}, rising to a maximum of 428 mAh g^{-1}, and finally maintaining 96.7% of its original capacity after 100 cycles.

Acknowledgments

This work was supported by National Science Foundation award (1632899 and 1332444) and University of Wyoming School of Energy Resources via the Carbon Engineering Initiative. J D S, J W, B Z, and F L acknowledge the Department of Chemistry Startup Funds at Virginia Tech.

ORCID iDs

Qilin Dai https://orcid.org/0000-0001-8680-4306

References

[1] Djurovic M, Oszajca M, Stochel G and van Eldik R 2018 The influence of redox-active transition metal containing micro-and nano-particles on the properties of representative bioinorganic reaction systems *European Journal of Inorganic Chemistry* (https://doi.org/10.1002/ejic.201701421)
[2] He Y, Xu P, Zhang B, Du Y, Song B, Han X and Peng H 2017 Ultrasmall MnO nanoparticles supported on nitrogen-doped carbon nanotubes as efficient anode materials for sodium ion batteries *ACS Applied Materials & Interfaces* **9** 38401–8
[3] Pellerin M, Castaing V, Gourier D, Chanéac C and Viana B 2018 Persistent luminescence of metal transition (Co, Ni)-doped $ZnGa_2O_4$ nanophosphors for applications in the near-infrared range *International Society for Optics and Photonics* **10533** 1053321
[4] Reaz M 2017 *Multifunctional Transition Metal Oxide Core Shell Magnetic Nanoparticles* Missouri State University https://bearworks.missouristate.edu/theses/3131/
[5] Tabassum H, Zou R, Mahmood A, Liang Z, Wang Q, Zhang H, Gao S, Qu C, Guo W and Guo S 2018 A universal strategy for hollow metal oxide nanoparticles encapsulated into B/N Co-doped graphitic nanotubes as high-performance lithium-ion battery anodes *Adv. Mater.* **30** 1705441
[6] Wang Y, Wang L, Ma Z, Gao L, Yin X, Song A, Qin X, Shao G and Gao W 2018 3D-structured carbon-coated MnO/graphene nanocomposites with exceptional electrochemical performance for Li-ion battery anodes *Journal of Solid State Electrochemistry* **22** 2977–87
[7] Wei Y, Zi Z, Chen B, Zhao B, Zhu X, Liang C, Ma X and Dai J 2018 Facile synthesis of hollow MnO microcubes as superior anode materials for lithium-ion batteries *J. Alloys Compd.* **756** 93–102
[8] Ilyasov V, Meshi B, Ryzhkin A, Ershov I, Nikiforov I and Ilyasov A 2011 Materials for spintronics: magnetic and transport properties of ultrathin (monolayer graphene)/MnO (001) and MnO (001) films *Journal of Modern Physics* **2** 1120
[9] Liu P P, Yang L Y, Liu W, Zhang Y, Wang H L, Liu S, Yang R R, Guo Y Q and Cui Y P 2018 Novel hybrid anode of MnO nanoparticles and ultrathin carbon sheets for high lithium storage performance *J. Alloys Compd.* **740** 375–81
[10] Jankovský O, Sedmidubský D, Šimek P, Sofer Z, Ulbrich P and Bartůněk V 2015 Synthesis of MnO, Mn_2O_3 and Mn_3O_4 nanocrystal clusters by thermal decomposition of manganese glycerolate *Ceram. Int.* **41** 595–601
[11] Schladt T D, Schneider K, Shukoor M I, Natalio F, Bauer H, Tahir M N, Weber S, Schreiber L M, Schröder H C and Müller W E 2010 Highly soluble multifunctional MnO nanoparticles for simultaneous optical and MRI imaging and cancer treatment using photodynamic therapy *J. Mater. Chem.* **20** 8297–304
[12] Shin J, Anisur R M, Ko M K, Im G H, Lee J H and Lee I S 2009 Hollow manganese oxide nanoparticles as multifunctional agents for magnetic resonance imaging and drug delivery *Angewandte Chemie International Edition* **48** 321–4
[13] Xu J-J, Zhao W, Luo X-L and Chen H-Y 2005 A sensitive biosensor for lactate based on layer-by-layer assembling MnO_2 nanoparticles and lactate oxidase on ion-sensitive field-effect transistors *Chemical Communications* **2005** 792–4
[14] Chang Y, Yu D P, Wang Z, Long Y, Zhang H and Ye R 2005 Fabrication and abnormal magnetic properties of MnO nanoparticles via vapor phase growth *J. Cryst. Growth* **281** 678–82
[15] Mutin P H and Vioux A 2009 Nonhydrolytic processing of oxide-based materials: simple routes to control homogeneity, morphology, and nanostructure *Chem. Mater.* **21** 582–96

[16] Yue J, Gu X, Chen L, Wang N, Jiang X, Xu H, Yang J and Qian Y 2014 General synthesis of hollow MnO_2, Mn_3O_4 and MnO nanospheres as superior anode materials for lithium ion batteries *J. Mater. Chem* A **2** 17421–6
[17] Li Q, Wang Z-L, Li G-R, Guo R, Ding L-X and Tong Y-X 2012 Design and synthesis of MnO_2/Mn/MnO_2 sandwich-structured nanotube arrays with high supercapacitive performance for electrochemical energy storage *Nano Lett.* **12** 3803–7
[18] Park J, Kang E, Bae C J, Park J-G, Noh H-J, Kim J-Y, Park J-H, Park H M and Hyeon T 2004 Synthesis, characterization, and magnetic properties of uniform-sized MnO nanospheres and nanorods *The Journal of Physical Chemistry* B **108** 13594–8
[19] Lin C-C, Chen C-J and Chiang R-K 2012 Facile synthesis of monodisperse MnO nanoparticles from bulk MnO *J. Cryst. Growth* **338** 152–6
[20] Lee G H, Huh S H, Jeong J W, Choi B J, Kim S H and Ri H-C 2002 Anomalous Magnetic Properties of MnO Nanoclusters *J. Am. Chem. Soc.* **124** 12094–5
[21] Zhang H, Jing L, Zeng J, Hou Y, Li Z and Gao M 2014 Revisiting the coordination chemistry for preparing manganese oxide nanocrystals in the presence of oleylamine and oleic acid *Nanoscale* **6** 5918–25
[22] Thackeray M M 1997 Manganese oxides for lithium batteries *Prog. Solid State Chem.* **25** 1–71
[23] Idota Y M M, Miyaki Y, Kubota T and Miyasaka T 1995 *Nonaqueous Secondary Batter. ed F P F C Ltd* Canadian Patent Applicationhttps://patents.google.com/patent/US5595841
[24] Zhang Y, Han F, Dai Q and Tang J 2018 Magnetic properties and photovoltaic applications of ZnO:Mn nanocrystals *J. Colloid Interface Sci.* **517** 194–203
[25] Zhang Y, Rimal G, Tang J and Dai Q 2018 Synthesis of $NiFe_2O_4$ nanoparticles for energy and environment applications *Mater. Res. Express* **5** 025023
[26] Xu Z, Shen C, Hou Y, Gao H and Sun S 2009 Oleylamine as both reducing agent and stabilizer in a facile synthesis of magnetite nanoparticles *Chem. Mater.* **21** 1778–80
[27] Morales M, Skomski R, Fritz S, Shelburne G, Shield J E, Yin M, O'Brien S and Leslie-Pelecky D 2007 Surface anisotropy and magnetic freezing of MnO nanoparticles *Phys. Rev* B **75** 134423
[28] Seo W S, Jo H H, Lee K, Kim B, Oh S J and Park J T 2004 Size-dependent magnetic properties of colloidal Mn_3O_4 and MnO nanoparticles *Angewandte Chemie International Edition* **43** 1115–7
[29] Bhide V and Dani R 1961 Electrical conductivity in oxides of manganese and related compounds *Physica* **27** 821–6